Journal of ELECTRONIC MATERIALS, Vol. 49, No. 4, 2020
https://doi.org/10.1007/s11664-020-07961-x

Temperature Dependence of Raman and Photoluminescence Spectra of Ternary Alloyed $CdSe_{0.3}Te_{0.7}$ Quantum Dots

LE XUAN HUNG,[1] PHAM THU NGA,[2,3] NGUYEN NHU DAT,[2,4] and NGUYEN THI THUC HIEN[2,5]

1.—Institute of Research and Development, Duy Tan University, 3 Quang Trung, Da Nang 550000, Vietnam. 2.—Institute of Theoretical and Applied Research, Duy Tan University, 1 Phung Chi Kien, Hanoi 100000, Vietnam. 3.—Institute of Materials Science, VAST, 18 Hoang Quoc Viet, Hanoi 100000, Vietnam. 4.—Institute of Physics, VAST, 18 Hoang Quoc Viet, Hanoi 100000, Vietnam. 5.—e-mail: hien49@gmail.com

The Raman and photoluminescence spectra of ternary alloyed $CdSe_{0.3}Te_{0.7}$ quantum dots (QDs) have been studied at temperatures between 84 K and 293 K. The average diameter of QDs is about 5.1 nm. The temperature dependence of the longitudinal optical (LO) phonon frequencies and the phonon band width was analyzed and the anharmonic constants relating to various high-order phonon processes was determined. While the three-phonon processes plays a dominant role in the temperature-dependent shift of the LO-phonon frequencies, the four-phonon processes contribute to the increase of the phonon linewidth with increasing temperature. The photoluminescence (PL) spectra were used to study the temperature dependence of the bandgap, the linewidth and the integrated PL intensity. At low temperatures below about 120 K, the PL linewidth decreases and the PL intensity increases as temperature increases. This temperature behavior can be ascribed to the exciton fine structure.

Key words: Raman scattering, photoluminescence, anharmonicity, exciton fine structure, phonon

INTRODUCTION

Alloy quantum dots are attractive because of their potential applications in optoelectronics. The advantage of alloy quantum dots (QDs) is the possibility to change, among various physical properties, the optical properties of the materials by controlling the composition and/or the size of the QDs. In addition, alloy QDs have good photochemical stability, higher crystallinity and high photoluminescent quantum yields.[1] Ternary alloyed $CdSe_{1-x}Te_x$ (abbreviated as CdSeTe) exhibits a so-called bowing effect, i.e., the plot of the band gap versus the composition is concave upwards. Therefore, the band gap of CdSeTe can be smaller than that of constituent binary parents CdSe and CdTe.[2] Thanks to the bowing effect, the light absorption range of CdSeTe can be shifted to the near-infrared region. This property can be exploited for construction of solar cells and near-infrared luminescent probers for *in vivo* molecular imaging and biomarker detection etc. Recently, Zou et al.[3] proposed the development of temperature-independent quantum dot light-emitting diodes (QLEDs) based on $CdSe_{1-x}Te_x$ alloyed QDs. By changing the Se-to-Te molar ratio of CdSeTe alloyed QDs, the energy levels of alloyed QDs can be adjusted so that the decrease in emission energy due to temperature-dependent lattice dilation will be offset by the increase in emission energy of trap-related exciton recombination. Thus, the quantum dots with temperature-independent emission peak can be produced.

Raman (RS) and photoluminescence (PL) spectroscopy are important tools to study the physical properties of materials samples, namely

(Received August 16, 2019; accepted January 13, 2020; published online January 30, 2020)

semiconductor QDs. It is known that when the temperature is changed, Raman and PL spectra also change. These changes are the shift in the line position, the change of the linewidth and the intensity. These changes are used for investigation of the vibrational and optical properties, e.g., the confinement effect on phonon and charge carrier structures,[4] electron/exciton–phonon interactions.[5] Furthermore, Raman and PL measurements have advantages that they are fast, sensitive and nondestructive means for investigation of crystallinity, electronic properties and so on.

In existing literature, to the best of our knowledge, there are no reports on the temperature dependence of Raman and PL spectra of alloyed CdSeTe QDs. Talwar et al.[6] reported on low-temperature (80 K) Raman scattering of bulk CdSeTe alloy. The authors of Ref. 7 revealed the possibility to determine the composition for CdSeTe nanocrystals embedded in glass by using Raman measurements.

In the present work, we have used the temperature dependence of Raman and PL spectra to investigate alloyed $CdSe_{0.3}Te_{0.7}$ QDs. The temperature range is from 84 K to 293 K. We used the Raman spectra to determine the anharmonicity of the sample. The temperature dependence of the band gap has been obtained by fitting the PL signals. The variation with temperature of the full width at half maximum (FWHM) of the PL spectra was also studied. We found that the PL intensity increases when the temperature increases from 84 to about 120 K. Then, it decreases with increasing temperature as expected. The increase of the PL intensity with increasing temperature at low temperatures was also observed in several semiconductors nanocrystals such as CdSe QDs,[8] CdTe QDs[9] and PbSe QDs.[10] It is suggested that this low-temperature behavior is coming from the exciton fine structure or the dark-bright exciton splitting, i.e., the splitting of the exciton level into dark exciton and bright exciton by electron-hole exchange interaction. The increase of the PL intensity is due to the transition from dark state to bright state. This is also attributed to some ligands on the surface of QDs.[11]

EXPERIMENT

The preparation of $CdSe_{1-x}Te_x$ ternary alloyed QDs has been described in our previous publications.[12,13] Therefore, we will give a brief description in the following.

The precursors included cadmium acetate dehydrate ($Cd(Ac)_2 \cdot 2H_2O$), selenium powder, and tellurium powder as sources of Cd, Se and Te, respectively. Oleic acid (OA) was used as surface ligands and 1-octadecene (ODE) and trioctylphosphine (TOP) as the reaction medium. After careful investigation[13] we have found out the best conditions for the synthesis: the growth temperature is 260°C, the growth time is 10 min. The growth temperature of 260°C has been chosen since it allows the best incorporation of both Te and Se into alloyed CdSeTe QDs.

CHARACTERIZATION

The QD samples were analyzed by micro-Raman spectroscopy (XploRA-Horiba). The excitation was performed by using a solid state laser with excitation line at 532 nm (25 mW). The laser power was 100 mW. The spot size of the laser beam was 1 μm. The spectral resolution was 2 cm^{-1}. The acquisition time ranged from 30 s to 120 s, but normally was 30 s. A charge coupled device (CCD) with four gratings with 600 slits/mm, 1200 slits/mm, 1800 slits/mm and 2400 slits/mm was used for detecting signals. The measuring range was from 100 cm^{-1} to 4000 cm^{-1}. We used the combination of the Raman XploRA Plus system with the THMS 600 Linkam temperature control system to carry out Raman and PL measurements at low temperatures from 84 K to 293 K. The Lynksys-32 sofware with temperature adjustment of 0.1 K was applied to control the THMS 600 system. A Xenon 450 W light with excitation wavelength selected at 532 nm was used for PL measurements. Transmission electron microscopy (TEM) measurements were carried out using a JEOL Jem 1010 microscope operating at 100 kV.

The TEM images of the CdTeSe QD samples have been presented in Ref. 13. The average QD size of 5.1 nm was determined from the obtained TEM images. The PL quantum yield of the samples reached a value of 24.9%. The powder x-ray diffraction (XRD) patterns and Raman analysis showed the alloy structure of the QDs. The QDs composition $x = 0.7$ was obtained from Raman spectra.[7] For all samples, the crystal lattice was found to be of zincblende structure.

RESULTS AND DISCUSSION

Temperature-Dependent Raman Shifts and FWHM

The Raman spectra of alloyed $CdSe_{1-x}Te_x$ QDs with $x = 0.7$ at different temperatures from 84 K to

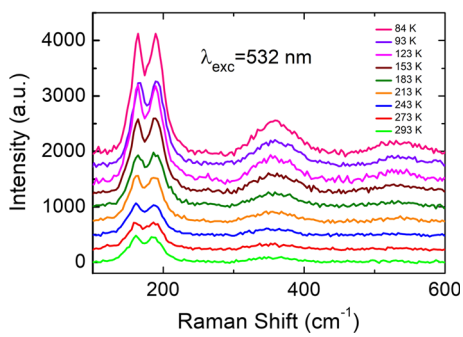

Fig. 1. Raman spectra of alloyed $CdSe_{0.3}Te_{0.7}$ QDs measured at temperature range from 84 K to 293 K.

293 K is shown in Fig. 1. It is clearly seen from the figure that, similar to bulk CdSeTe, the Raman spectra of CdSeTe QDs exhibit a two-mode behavior, i.e., show both a "CdTe-like" mode (denoted by LO_1) and a "CdSe-like" mode (denoted by LO_2) of optical phonon frequencies at about 160 cm^{-1} and 190 cm^{-1}, respectively. It is noted that the longitudinal optical (LO) phonon frequency is about 170 cm^{-1} for bulk CdTe and 210 cm^{-1} for bulk CdSe. Furthermore, as the temperature increases, the phonon frequencies are shifted to lower region, showing a redshift. Meanwhile, the intensities decrease, the linewidths increase and the peaks in the spectra are less pronounced. At low temperatures, broad side bands appear at higher frequency, showing the contribution of higher (the second and the third) order processes.

The temperature dependence of Raman frequencies and linewidths in a bulk semiconductor was studied by Balkanski et al.[14] They explained this temperature dependence by the anharmonicity in the vibrational potential, which leads to decay of the zone-center optical phonon into two, three or more phonons without or with absorption of another phonon, corresponding to cubic, quartic or higher order anharmonicities. In nanocrystals, the q-vector selection rule may relax, which enhances these phonon couplings and changes the temperature dependence of Raman frequencies and linewidths.

According to Balkanski et al.,[14] the temperature dependence of the phonon frequency $\omega(T)$ and the linewidth $\Gamma(T)$ of the phonon LO mode at the center of the Brillouin zone can be written as $\omega(T) = \omega_0 + \Delta\omega(T)$ and $\Gamma(T) = \Gamma_0 + \Delta\Gamma(T)$ with

$$\Delta\omega(T) = A\left[1+\frac{2}{e^x-1}\right] + B\left[1+\frac{3}{e^y-1}+\frac{3}{(e^y-1)^2}\right], \tag{1}$$

$$\Delta\Gamma(T) = C\left[1+\frac{2}{e^x-1}\right] + D\left[1+\frac{3}{e^y-1}+\frac{3}{(e^y-1)^2}\right]. \tag{2}$$

Here $x = (\hbar\omega_0/(2k_BT))$, $y = (\hbar\omega_0/(3k_BT))$, ω_0 and Γ_0 are the intrinsic frequency and linewidth of the LO-phonon mode, respectively, A, B, C and D are different anharmonic constants. Γ_0 is related to the natural lifetime of the Raman intermediate excited vibrational state.[15] Collecting the constants we obtain

$$\begin{aligned}\omega(T) &= \omega_0 + A + B \\ &\quad + A\left[\frac{2}{e^x-1}\right] + B\left[\frac{3}{e^y-1}+\frac{3}{(e^y-1)^2}\right] \\ &\equiv \omega^* + A\left[\frac{2}{e^x-1}\right] + B\left[\frac{3}{e^y-1}+\frac{3}{(e^y-1)^2}\right],\end{aligned} \tag{3}$$

$$\begin{aligned}\Gamma(T) &= \Gamma_0 + C + D \\ &\quad + C\left[\frac{2}{e^x-1}\right] + D\left[\frac{3}{e^y-1}+\frac{3}{(e^y-1)^2}\right] \\ &\equiv \Gamma^* + C\left[\frac{2}{e^x-1}\right] + D\left[\frac{3}{e^y-1}+\frac{3}{(e^y-1)^2}\right].\end{aligned} \tag{4}$$

ω^* and Γ^* are the Raman frequency and the linewidth in the harmonic limit, respectively. The second term in rhs of Eqs. 3 and 4 describes three-phonon processes and the last one describes four-phonon processes. Since A, B are much smaller than ω_0 so that $\omega^* \sim \omega_0$. When the experimental temperature is not high (in comparison with the Debye temperature of materials under consideration), high order processes can be neglected. It is worth noting that for alloys, the anharmonicity is shown to be dependent on composition.[16]

The relations 3 and 4 are applicable to both CdTe-like and CdSe-like modes.

It is difficult to assess the linewidth data since there are some factors that affect the width of Raman lines: disorder in alloys (giving rise to asymmetric broadening which is independent of temperature), anharmonic decay of phonons, inhomogeneity in nanoparticle size, finite resolution of the spectrometer.

For fitting the data of line peaks and linewidths of Raman spectra obtained for TiO_2 nanocrystals, Zhu et al.[17] calculated the Raman intensity profile using the Lorentzian function weighted by a Gaussian function to take into account the contribution of off-center phonons. Kush et al.[18] used the sum of two Lorentzian functions to fit the asymmetric shape of the fundamental Raman line of CdSe QDs and considered it to be due to contribution from two optical phonon modes—LO and SO (surface optical) modes. In our case, in order to distinguish overlapping asymmetric lines corresponding to LO_1 and LO_2 modes, we have fitted the experimental Raman spectra using a Gauss-Lorentzian function available

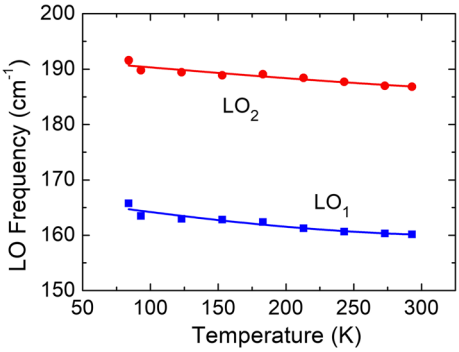

Fig. 2. Temperature variation of CdTe-like (LO_1) and CdSe-like (LO_2) mode frequencies of alloyed CdSeTe QDs. The dots are experimental values and solid lines are the fitted curves.

Table I. Best fit parameters for temperature dependence of LO frequency according to Eq. 3

Phonon mode	ω_0 (cm^{-1})	A (cm^{-1})	B (cm^{-1})
LO_1 (CdTe-like)	169	3.06	0.15
LO_2 (CdSe-like)	193	2.0	0.07

in labspec software. The temperature dependence of CdTe-like mode and CdSe-like mode frequencies is displayed in Fig. 2. Solid lines in the figure are the fits to experimental data according to Eq. 3.

The best fit values of the intrinsic frequency ω_0 and of paremeters A and B are shown in Table I for both LO_1 and LO_2 modes. The value of ω_0 for CdTe-like LO phonon mode in CdTeSe QDs is 169 cm^{-1}, meanwhile the bulk CdTe value is 170–173 cm^{-1}.[19] ω_0 for CdSe-like mode is 193 cm^{-1} in alloy QDs and 215 cm^{-1} in bulk CdSe.[20] Our values of ω_0 are smaller than that in bulk samples. This is attributed to phonon confinement effect.[21]

Concerning the anharmonic constants A, B in Eq. 3 and C, D in Eq. 4, we will compare our results with that in the case of composition limits, i.e., when $x = 1$ (CdTe) and $x = 0$ (CdSe). Kush et al.[18] obtained $A = 4.2\,cm^{-1}$, $B = 2.1\,cm^{-1}$ for CdSe QDs with diameter of 4.8 nm and $A = 5.2\,cm^{-1}$, $B = 0.8\,cm^{-1}$ for 6 nm diameter QDs. These values of A and B are larger than that for CdSe-like (LO_2) phonon mode in our case (alloyed CdTeSe QDs with 5.1 nm average diameter). The authors also obtained $A = 47.1\,cm^{-1}$, $B = 0.0018\,cm^{-1}$ for bulk CdSe. Stergiou et al.[22] obtained $A = 1.11\,cm^{-1}$ for bulk CdTe, neglecting the four-phonon processes in Eq. 3. These values are smaller than that of our CdTe-like (LO_1) mode. It is hard to give any explanation to the results.

The temperature dependence of the full width at half maximum of LO phonon bands (LO FWHM) for alloyed CdSeTe QD samples is depicted in Fig. 3 along with the fit according to Eq. 4. As reported in Ref. 18, the LO FWHM is 10–20 cm^{-1} in the temperature range 80–300 K for binary CdSe QDs. This value is 2–5 cm^{-1} for bulk CdTe.[22] Meanwhile, as seen from Fig. 3, the LO FWHM is of 20–30 cm^{-1} for alloyed CdSeTe QDs in the same temperature range, i.e., is much larger than that reported in Refs. 18 and 22. When the temperature increases, the lifetime of the Raman intermediate state decreases, resulting in the broadening of the Raman line according to the Heisenberg uncertainty principle. The anharmonic terms in Eq. 4 give rise to linear and quadratic variation in temperature dependence of the linewidth at high temperature.

The best fitting anharmonic constants C and D are shown in Table II. For bulk CdTe, Stergiou et al.[22] obtained $C = 0.88\,cm^{-1}$, taking into account only three-phonon processes in Eq. 4. In the same approximation, the value of $C = 0.006\,cm^{-1}$ was

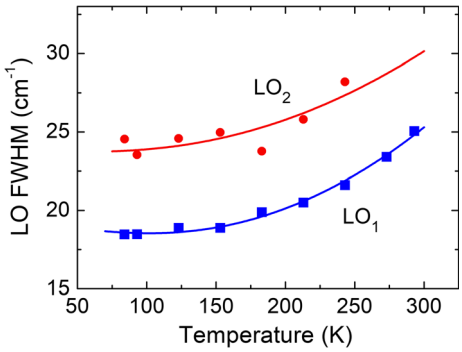

Fig. 3. Temperature dependence of LO FWHM for CdSeTe QDs. The dots are the experimental values. Solid lines are the fits to experimental data.

Table II. Anharmonic constants obtained by fitting Eq. 4 to the experimental temperature-dependent linewidth

LO phonon mode	C (cm^{-1})	D (cm^{-1})
LO_1 (CdTe-like)	2.70	0.43
LO_2 (CdSe-like)	1.48	0.36

Table III. Ratio between anharmonic constants

LO phonon mode	B/A	D/C
LO_1 (CdTe-like)	0.05	0.16
LO_2 (CdSe-like)	0.035	0.24

reported for bulk CdSe in Ref. 18 by Kusch and co-authors. Compared to values of C given in Table II, one can see that the value of constant C for alloyed CdSeTe QDs is greater than that of bulk CdSe and CdTe, that means the anharmonicity is more effective in CdSeTe QDs than in bulk materials.

We have calculated the ratios of B/A and D/C for LO_1 and LO_2 modes in alloyed CdSeTe QDs. The results are presented in Table III. It is found that the contribution of the four-phonon processes is small compared to the three-phonon processes. Since the ratio B/A is much less than unity, we can assume that the LO phonon decay into two phonons is the main mechanism in the temperature dependent shift of the one-phonon Raman line centers, leading to the almost linear temperature-dependence of LO frequencies as seen in Fig. 2. As concerns the linewidth, although the ratio D/C is less than unity but not as high as the ratio B/A, one can expect that the four-phonon term in Eq. 4 still contributes and gives rise to the non-linear temperature dependence of the linewidth at high temperature. This is reflected in Fig. 3.

Because of the existence of two-mode phonons, CdSe-like and CdTe-like LO phonons, in ternary alloyed $CdSe_{1-x}Te_x$ QDs, it would be useful to introduce an average LO-phonon energy E_{LO}

related to an effective LO-phonon frequency $\langle\omega_{LO}\rangle(x)$ defined as (following Eq. (16) in Ref. 23)

$$\langle\omega_{LO}\rangle(x) = (1-x)\,\omega_{LO}^{CdSe}(x) + x\,\omega_{LO}^{CdTe}(x) \qquad (5)$$

where $\omega_{LO}^{CdSe}(x)$ and $\omega_{LO}^{CdTe}(x)$ are frequencies of CdSe-like and CdTe-like LO phonon modes, respectively, in $CdSe_{1-x}Te_x$ QDs. Using data in Table I we obtained $E_{LO} = 21.8$ meV for $CdSe_{1-x}Te_x$ QDs with $x = 0.7$.

Temperature-Dependent Photoluminescence

Figure 4 shows the temperature-dependent PL spectra for ternary alloyed $CdSe_{1-x}Te_x$ QDs ($x = 0.7$). The temperature range is from 84 K to 293 K. It is seen that the curves differ slightly from symmetric line shapes, especially at high temperatures. Therefore, instead of using a symmetric Gaussian or Lorentzian function to fit the spectra to obtain the peak parameters we took a function $f(\omega)$ introduced by Korepanov et al.[24]

$$f(\omega) = m\frac{A}{\Gamma}\sqrt{\frac{4\ln 2}{\pi}}\exp\left[-4\ln 2\left(\frac{\omega\times p(\omega)-\omega_0}{\Gamma}\right)^2\right] + (1-m)\frac{A}{2\pi}\frac{\Gamma}{(\omega\times p(\omega)-\omega_0)^2+\left(\frac{\Gamma}{2}\right)^2} \qquad (6)$$

with

$$p(\omega) = 1 - a\times\frac{\omega-\omega_0}{\Gamma}\times\exp\left[-\frac{(\omega-\omega_0)^2}{2(2\Gamma)^2}\right] . \qquad (7)$$

Here ω_0 is the peak frequency, Γ is the full width at half maximum, A is the peak area, a is the asymmetry parameter, and m is the fraction of the Gaussian contribution to the line shape.

Figure 5a displays 293 K PL spectrum and a fit to measured values using Eq. 6 with $m = 0.57$. For comparison, we plotted in Fig. 5b the fits by Gaussian and Lorentzian functions.

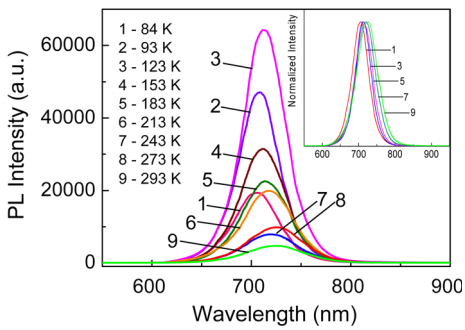

Fig. 4. PL spectra of CdSeTe QDs measured at different temperatures from 84 K to 293 K. Inset: normalized PL spectra.

Temperature Dependence of PL Peak Position

The PL peak energy variation with temperature is shown in Fig. 6 for CdSeTe QDs. As is well known, the PL peak energy represents the energy gap of the sample. Therefore, we can see from the figure how the band gap E_g of alloyed CdSeTe QDs changes with varying temperature. The fit to the experimental PL maximum for different fitting models is also displayed in Fig. 6.

As seen in Fig. 6, the QD energy gap shows a redshift of about 48 meV when the temperature increases from 84 K to 293 K. The redshift reflects a shrink of the band gap with increasing temperature due to exciton-phonon interaction as suggested by Wan et al.[25] Based on the assumption about two mechanisms of variation in energy gap with temperature, the thermal expansion of the lattice and the temperature dependent electron-phonon interaction, Varshni[26] proposed the following relation to describe the temperature dependence of the energy gap

$$E_g(T) = E_g(0) - \frac{\alpha T^2}{T+\beta} \qquad (8)$$

where $E_g(0)$ is the band gap at $T = 0$ K, α is a parameter associated with lattice expansion due to temperature changes, β is a constant of the order of the Debye temperature Θ_D of the material considered and related to electron-phonon interaction. The Varshni relation 8 is originally applied for bulk semiconductors but it is found to be valid for quantum dots as well.[27] α and β vary with the size and the composition of QDs.

We employ the Varshni model to analyze the variation with temperature in PL spectra of alloyed CdSeTe QDs in the temperature range 150–300 K. It is noted that the band gap $E_g(0)$ is now the sum of the $T = 0$ bulk band gap and the quantum confinement energy E_{conf} of the QD. The fit using Eq. 8 is displayed in Fig. 6a as solid line. The related fitting parameters are given in Table IV.

The band gap $E_g(0)$ at 0 K for bulk CdTe and CdSe is 1.61 eV and 1.84 eV, respectively.[28] Following Singh et al.[29] we have calculated the effective band gap of corresponding QDs and obtained 1.79 eV for CdTe QDs, 2.03 eV for CdSe QDs, both with the average diameter of 5.1 nm. The band gap of ternary alloyed $CdSe_{1-x}Te_x$ QDs at $T = 0$ K can be evaluated using the formula

$$E_g^{CdSeTe}(0) = xE_g^{CdTe}(0) + (1-x)E_g^{CdSe}(0) - b(1-x)x \qquad (9)$$

where b is the bowing factor which is taken as 0.75 for $x = 0.7$.[30] The calculated $E_g(0)$ for alloyed CdSeTe QDs is 1.71 eV in good agreement with the fitting value of 1.763 eV (see Table IV).

We obtained the best fit value of 2.6×10^{-4} eV K^{-1} for α which is very close to the value

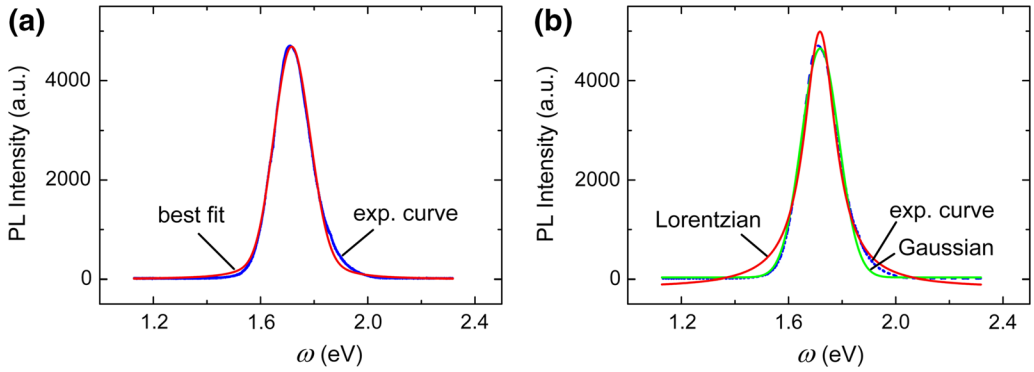

Fig. 5. PL spectrum of CdSeTe QDs at 293 K and the best fits using (a) function (6) suggested by Korepanov et al. and (b) symmetric Gaussian and Lorentzian functions.

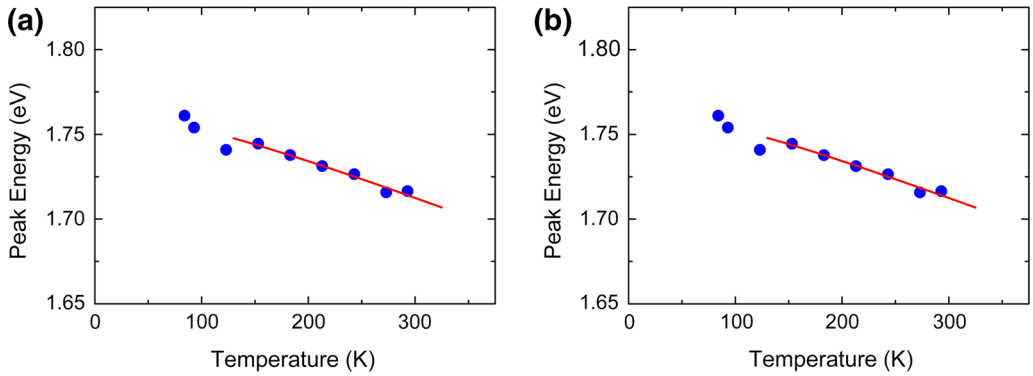

Fig. 6. PL peak energy vs temperature for alloyed CdSeTe QDs. The solid lines are theoretical fits using (a) Varshni relation (Eq. 8) and (b) O'Donnell and Chen relation (Eq. 10). The dots are the experimental data.

Table IV. Parameters extracted from fitting to the Varshni relation (Eq. 8)

$E_g(0)$ (eV)	α (10^{-4} eV K^{-1})	β (K)
1.763	2.6	162

of 3×10^{-4} eV K^{-1} for bulk CdTe[5] and $(2.8–4.1) \times 10^{-4}$ eV K^{-1} for bulk CdSe.[31] For the constant β we got a value of 162 K compared to the Debye temperature Θ_D of 155–170 K for bulk CdTe[6] and 181–315 K for bulk CdSe.[31] The results show that the temperature dependence of the band gap of QDs is similar to that of the bulk in the temperature range considered.

O'Donnell and Chen[32] claimed that the Varshni model does not accurately predict the low-temperature behavior of the band gap and the sign of constant β in some cases. They proposed the equation describing temperature dependence of band gap

$$E_g(T) = E_g(0) - S E_{LO}\left[\coth\left(\frac{E_{LO}}{2k_B T}\right) - 1\right] \qquad (10)$$

in which the fitting parameters are related to intrinsic electron-phonon interaction of materials. Here E_{LO} is the average phonon energy (see Eq. 5),

Table V. Parameters obtained from the temperature-dependent energy gap, fitted by the O'Donnel and Chen relation (Eq. 10)

$E_g(0)$ (eV)	S	E_{LO} (meV)
1.756	1.38	21.9

S is the dimensionless coupling constant (referred to as Huang-Rhys parameter) describing the strength of electron-phonon coupling.[33]

We utilized Eq. 10 to fit the PL peak position for alloyed CdSeTe QDs for temperature from 150 to 300 K and depicted the fit in Fig. 6b as solid line. The fitting parameters are listed in Table V.

It is seen that the fitting value of the zero-temperature band gap $E_g(0)$ is the same as that obtained by the Varshni model. The average phonon energy $E_{LO} = 21.9$ meV is in good agreement with that of 21.8 meV calculated from Raman measurement data (see below Eq. 5).

There are some values of constant S reported for bulk CdTe, such as $S = 1.68$[34] and $S = 4.904$.[22] Jagtap et al.[35] reported the value of S from 1.13 to 1.53 for CdTe QDs capped with a CdS shell with size decreasing from 4.8 to 3.0 nm. For ternary alloyed $Cd_{0.8}Hg_{0.2}Te$ QDs, the value of S is 1.17–1.68 for

QDs with diameter of 2.5–4.2 nm but there is no trend in S with respect to the size of QDs.[36] The authors of Ref. 36 claimed this lack of trend is due to the broad size distribution and variation in the composition of the ternary alloyed QDs. The calculated value of the Huang-Rhys factor is $S \approx 10$ for bulk CdSe and the reported values for CdSe QDs are much smaller.[37] Our best fit value for parameter S for alloyed CdSeTe QDs is 1.38 which is between the values reported for CdSe and CdTe QDs.

As shown in Fig. 6, the PL peak position exhibits a blueshift when the temperature decreases from 300 to about 150 K. In further decrease in temperature, a redshift occurs at about 120 K and then the peak shifts to higher energy again. It is worth noting that a similar behavior was observed in the temperature-dependent emission from CdTe QDs which is attributed to exciton splitting.[9]

Temperature Dependence of the FWHM

The temperature dependence of the PL linewidth due to exciton scattering by acoustic and LO phonons can be described by the relation[38]

$$\Gamma(T) = \Gamma_{inh} + \gamma_{ac} T + \gamma_{LO} \left(e^{\frac{E_{LO}}{k_B T}} - 1 \right)^{-1} \qquad (11)$$

where Γ_{inh} is the inhomogeneous linewidth which results from fluctuation in size, shape, and composition of quantum dots and is temperature-independent (considered the linewidth at 0 K). The other terms describe the homogeneous broadening, in which the coefficients γ_{ac} and γ_{LO} are independent of temperature and characterize the linewidth due to the exciton-acoustic-phonon and exciton-LO-phonon interaction, respectively. E_{LO} is the average LO-phonon energy introduced by Eq. 5,

$$N_{LO}(T) = [\exp(E_{LO}/k_B T) - 1]^{-1} \qquad (12)$$

is the Bose-Einstein distribution of LO phonons. Equation 11 is initially applied to analyze the temperature variation of exciton luminescence linewidths in bulk semiconductors and then is also used for low-dimensional structures.[33] The FWHM of the PL spectra of alloyed CdSeTe QDs is depicted in Fig. 7 as a function of temperature and is fitted to Eq. 11. The best values of fitting parameters are tabulated in Table VI.

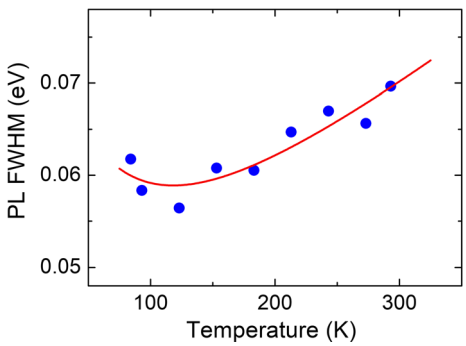

Fig. 7. Temperature dependence of PL FWHM for alloyed CdSeTe QDs with the average diameter of 5.1 nm. The dots are experimental values, the solid line is the fit to Eq. 11.

As pointed out in Ref. 39, the exciton–acoustic-phonon interaction plays a dominant role in the temperature dependence of the PL linewidth at temperatures less than 100 K. The authors of Ref. 36 reported the values of γ_{ac} which are 53.2 μeV K^{-1}, 53.5 μeV K^{-1}, and 54.4 μeV K^{-1} for $Cd_{0.8}Hg_{0.2}Te$ QDs with diameter of 2.5 nm, 2.9 nm, and 4.2 nm, respectively. Their results showed that the PL linewidth remains independent of temperature up to 70 K and then increases with increasing temperature in the case of QDs with 2.5 and 2.9 nm diameter. Meanwhile, the linewidth for 4.2 nm diameter QDs increases continuously over the temperature range from 15 to 300 K. The analysis of PL spectra of CdSe/ZnS core-shell QDs with an average radius of 2.5 nm gives a value of 71 μeV K^{-1} for parameter γ_{ac} which is two times larger than the calculated value for bare CdSe QDs.[38] For CdTe QDs, Morello and co-authors[5] found that the value of γ_{ac} is large, up to 31 μeV K^{-1}. It can be seen that the exciton-acoustic phonon coupling constant γ_{ac} of QDs is much greater than that of bulk samples (theoretical estimation of 0.7 μeV K^{-1} for bulk CdTe[39] and 8 μeV K^{-1} for bulk CdSe).[40] This is ascribed to the enhancement of exciton coupling with acoustic phonons in low-dimensional systems, indicating the effect of confinement.[38]

The plot in Fig. 7 shows two different dependencies of the linewidth on temperature: a high temperature slope and a low-temperature curvature. At high temperatures, the linewidth increases as the temperature increases as for most ordinary semiconductors, but in the temperature range from 80 to around 120 K, the linewidth decreases with increasing temperature. This linewidth narrowing at low temperature may be due to the transfer of excitons between dark and bright states within each QD of relatively large sizes as mentioned in Refs. 41–43. The mentioned temperature dependence of the linewidth is reflected by the negative sign of the extracted value of parameter γ_{ac}, $\gamma_{ac} = -240$ μeV K^{-1}. The absolute value of the fitting γ_{ac} is too large compared to the reported ones in literature, though a value of 380 μeV K^{-1} is obtained for CdSe platelets.[44] The temperature

Table VI. The best fit parameters for the temperature-dependent PL FWHM using Eq. 11

Γ_{inh} (meV)	γ_{ac} (μeV)	γ_{LO} (meV)	E_{LO} (meV)
75.8	− 240	90.1	21.97

behavior of the PL linewidth of the alloyed CdSeTe QDs needs some additional consideration.

Concerning the exciton–LO-phonon coupling, Rudin et al.[39] have calculated the linewidth due to the Fröhlich interaction of excitons with LO-phonons, including both exciton bound states and continuum ones. The correction coming from the resonant interaction between excitons and photons to form so called polaritons was also taken into account. They obtained values of 18.3 meV and 24.5 meV for constant γ_{LO} of bulk CdSe and CdTe, respectively. The experimental values for γ_{LO} are 53 meV and 35 meV for respective bulk CdSe and CdTe,[45] 207 meV for CdSe bulk material.[40] Morello et al.[5] utilized Eq. 11 to fit measured PL linewidths and obtained the best fit values 14 meV, 18.3 meV, and 21 meV of γ_{LO} for CdTe QDs with diameter of 4.2 nm, 4.9 nm, and 5.9 nm, respectively. Their results showed the exciton–LO-phonon coupling constant γ_{LO} of QDs is smaller than the bulk one and increases as the QDs diameter increases. This tendency of γ_{LO} for QDs can be ascribed to the overlap of electron and hole wave functions in the quantum confinement regime. Our extracted value of γ_{LO} is 90.1 meV, larger than most of available data for QDs but still smaller than the bulk value of 270 meV mentioned above for CdSe.

Temperature-Dependent PL Intensity

Figure 8 shows the temperature variation of the integrated PL intensity of alloyed CdSeTe QDs. As discussed in Ref. 36, the behavior of the PL temperature dependence suggests the existence of two types of nonradiative recombination processes (denoted by a and b). In this case, the temperature dependence of the integrated PL intensity can be described by the relation[36]

$$I_{PL}(T) = \frac{I_0}{1 + Ae^{-\frac{E_a}{k_B T}} + Be^{-\frac{E_b}{k_B T}}} \quad . \qquad (13)$$

where I_0 is the integrated PL intensity at 0 K, E_a and E_b are the activation energies associated with different nonradiative processes. A and B are constants defined as the ratios of the exciton radiative lifetime τ of QDs over the capture time of exciton τ_a and τ_b, respectively, by nonradiative recombination centers.

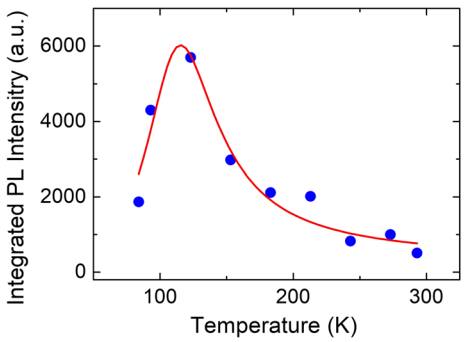

Fig. 8. Integrated PL intensity versus temperature of alloyed CdSeTe QDs. The dots are experimental values. The solid line is the fitting curve by Eq. 13.

We have used Eq. 13 to fit the experimental data. The best fit parameters are tabulated in Table VII.

The PL intensity does not change monotonously with temperature. In the temperature range below about 120 K, the intensity increases as temperature increases. Above 120 K, the intensity decreases with increasing temperature. A similar temperature dependence of PL intensity is also observed in CdTe nanocrystals,[9] CdSe QDs,[37] CdSe/ZnS core-shell QDs,[11] and CdSe QDs embedded in a CdS nanorod.[46] This behavior of the intensity variation with temperature is a feature of the strong confinement and is related to the so-called exciton fine structure. At lower temperatures, the thermally activated transfer of population from dark exciton state (optically forbidden) to bright exciton state (optically allowed) causes the increase of the emission intensity with increasing temperature. In the range of higher temperatures, nonradiative recombination is supported by the increase in phonon population, leading to the decrease of PL intensity. As reported in Ref. 9, the exciton energy splitting in zinc-blende CdTe nanocrystals is estimated to be 5 meV and 13 meV for QDs with diameter of 3.0 nm and 1.9 nm, respectively. Therefore, the PL intensity increases at low temperatures from 20 to about 40 K for 3.0 nm QDs and from 40 to 60 K for 1.9 nm QDs. For CdTe/CdS core-shell QDs with radii greater than 3 nm, the PL intensity increases in the range of temperature from 15 to 25 K and then decreases at temperatures above about 50 K.[47]

In accordance with the mentioned above, the nonradiative recombination process denoted by a is associated with interaction of excitons with LO-phonons. The obtained value of activation energy $E_a = 20.8$ meV is in good agreement with the average LO-phonon energy $E_{LO} = 21.8$ meV obtained from Raman measurements (see below Eq. 5). At low temperatures, the nonradiative recombination is due to exciton fine structure, i.e., the splitting of the exciton into dark exciton and bright exciton by the exchange interaction. The energy splitting is defined as activation energy E_b which is estimated to be 14.9 meV as described in Table VII. The PL is then expected to exhibit a decline at temperatures below 120 – 130 K. It should be noted that the energy difference between

Table VII. Best parameters obtained from the temperature-dependent integrated PL intensity fitted to Eq. 13

A	B	E_a (meV)	E_b (meV)
17.14	– 13.40	20.8	14.9

dark and bright exciton states is 13 meV in CdTe QDs with 1.9 nm diameter.[36]

The above explanation on the temperature behavior of the integrated PL intensity of alloyed CeSeTe QDs is supported by the temperature dependence of the PL linewidth depicted in Fig. 7 as discussed in the preceding Subsection.

The temperature dependence of the photoluminescence might be affected by several carrier relaxation mechanisms such as radiative recombination, nonradiative Auger processes, carrier trapping at surface trap states. This work is a preliminary study of photoluminescence of ternary alloyed CdSeTe Qds. For a deeper understanding, it needs supplementary measurements, e.g. photoluminescence decay.

CONCLUSION

In summary, we have studied the fundamental Raman band and photoluminescence properties of ternary alloyed $CdSe_{1-x}Te_x$ QDs ($x = 0.7$) in the temperature range from 84 K to 293 K. Various models have been used to understand the temperature dependence of Raman and photoluminescence characteristics of the samples. The Raman spectra of the samples display two distinct peaks, showing CdTe-like and CdSe-like LO-phonon modes. The temperature dependence of LO-phonon frequencies and the LO FWHM exhibits the anharmonic effect. The decay of the zone-center LO phonon into two phonons plays dominant role in the temperature-dependent shift of the LO-phonon frequencies, meanwhile the four-phonon processes contribute to the non-linear temperature dependence of the LO-phonon band width. The average LO-phonon energy is introduced and has a value of 21.8 meV.

The temperature dependence of the QD band gap has been obtained from the variation of the PL peak position with temperature. The redshift of the band gap when temperature increases is related to the thermal expansion of the lattice and the change of electron-phonon coupling. A slight blueshift in the band gap at 120 – 150 K is ascribed to the exciton fine structure. The variation of the PL linewidth and integrated intensity with temperature of our alloyed CdSeTe QDs samples in the range of high temperature is similar to that of most semiconductors, that is, the linewidth increases and the intensity decreases with increasing temperature. Interaction of excitons with acoustic and LO phonons is responsible for such temperature dependence. At temperatures below about 120 K, the PL linewidth decreases, and the PL intensity increases, when temperature increases. This anomalous behavior of the PL linewidth and intensity can be attributed to the transfer of excitons between dark and bright states within a QD itself.

ACKNOWLEDGMENTS

This research is funded by the Vietnam National Foundation for Science and Technology Development (NAFOSTED) under Grant No. 103.03-2018.03. The authors also thank the National Key Laboratory for Electronic Materials and Devices (IMS) and Duy Tan University for giving facilities to cary out the research.

REFERENCES

1. X. Zhong, M. Han, Z. Dong, T.J. White, and W. Knoll, *J. Am. Chem. Soc.* 125, 8589 (2003).
2. R.E. Bailey and S. Nie, *J. Am. Chem. Soc.* 125, 7100 (2003).
3. H. Zou, M. Liu, D. Zhou, X. Zhang, Y. Liu, B. Yang, and H. Zhang, *J. Phys. Chem. C* 121, 5313 (2017).
4. Z.D. Fu, Y.S. Cui, S.Y. Zhang, J. Chen, D.P. Yu, and S.L. Zhang, *Appl. Phys. Lett.* 90, 263113 (2007).
5. G. Morello, M. De Giorgi, S. Kudera, L. Manna, R. Cingolani, and M. Anni, *J. Phys. Chem. C* 111, 5846 (2007).
6. D.N. Talwar, Z.C. Feng, J.-F. Lee, and P. Becla, *Phys. Rev. B* 87, 165208 (2013).
7. Y.I. YuM Azhniuk, V.V. Hutych, L.A. Lopushansky, A.V. Prots, and B.R.T.Z. Gomonnai, *Phys. Status Solidi C* 6, 2064 (2009).
8. S.A. Crooker, T. Barrick, J.A. Hollingsworth, and V.I. Klimov, *Appl. Phys. Lett.* 82, 2793 (2003).
9. Y. Nonoguchi, T. Nakashima, and T. Kawai, *J. Phys. Chem. C* 111, 11811 (2007).
10. E. Lifshitz, R. Vaxenburg, G.I. Maikov, D. Yanover, A. Brusilovski, J. Tilchin, and A. Sashchiuk, in *Semiconductors and Semimetals, Quantum Efficiency in Complex Systems, Part II: From Molecular Aggregates to Organic Solar Cells*, vol. 85, ed. by U. Würfel, M. Thorwart, E.R. Weber (Elsevier, San Diego, 2011), p. 181.
11. P. Jing, J. Zheng, M. Ikezawa, X. Liu, S. Lv, X. Kong, J. Zhao, and Y. Masumoto, *J. Phys. Chem. C* 113, 13545 (2009).
12. L.X. Hung, P.N. Thang, H.V. Nong, N.H. Yen, V.D. Chinh, L.V. Vu, N.T.T. Hien, W.D. de Marcillac, P.N. Hong, N.T. Loan, C. Schwob, A. Maître, N.Q. Liem, P. Bénalloul, L. Coolen, and P.T. Nga, *J. Electron. Mater.* 45, 4425 (2016).
13. L.X. Hung, P.D. Bassène, P.N. Thang, N.T. Loan, W.D. de Marcillac, A.R. Dhawan, F. Feng, J.U. Esparza-Villa, N.T.T. Hien, N.Q. Liem, L. Coolen, and P.T. Nga, *RSC Adv.* 7, 47966 (2017).
14. M. Balkanski, R.F. Wallis, and E. Haro, *Phys. Rev. B* 28, 1928 (1983).
15. H.W. Nesbitt, G.M. Bancroft, and G.S. Henderson, *Am. Mineral.* 103, 966 (2018).
16. R. Beserman, C. Hirliman, M. Balkanski, and J. Chevallier, *Solid State Commun.* 20, 485 (1976).
17. K.-R. Zhu, M.-S. Zhang, Q. Chen, and Z. Yin, *Phys. Lett. A* 340, 220 (2005).
18. P. Kusch, H. Lange, M. Artemyev, and C. Thomsen, *Solid State Commun.* 151, 67 (2011).
19. V. Dzhagan, M.Y. Valakh, J. Kolny-Olesiak, I. Lokteva, and D.R.T. Zahn, *Appl. Phys. Lett.* 94, 243101 (2009).
20. M. Mohr and C. Thomsen, *Nanotechnology* 20, 115707 (2009).
21. A.G. Rolo and M.I. Vasilevskiy, *J. Raman Spectrosc.* 38, 618 (2007).
22. V.C. Stergiou, A.G. Kontos, and Y.S. Raptis, *Phys. Rev. B* 77, 235201 (2008).
23. S. Adachi, *J. Appl. Phys.* 58, R1 (1985).
24. V.I. Korepanov and D.M. Sedlovets, *Analyst* 143, 2674 (2018).
25. J.Z. Wan, J.L. Brelinar, R. Leonelli, G. Zhao and J.T. Graham, *Phys. Rev. B* 48, 5197 (1993).
26. Y.P. Varshni, *Physica* 34, 149 (1967).
27. I. Yeo, J.D. Song, and J. Lee, *Appl. Phys. Lett.* 99, 151909 (2011).

28. C. Kittel, *Introduction to Solid State Physics*, 8th edn. (Wiley, Hoboken, 2005), p. 190.
29. M. Singh, M. Goyal, and K. Devlal, *J. Taibah Univ. Sci.* 12, 470 (2018).
30. H. Asano and T. Omata, *AIP Adv.* 7, 045309 (2017).
31. Landolt-Börnstein, *Numerical Data and Functional Relationship in Science and Technology. Group III* (1982), p. 16.
32. K.P. O'Donnell and X. Chen, *Appl. Phys. Lett.* 58, 2924 (1991).
33. M.S. Gaponenko, A.A. Lutich, N.A. Tolstik, A.A. Onushchenko, A.M. Malyarevich, E.P. Petrov, and K.V. Yumashev, *Phys. Rev. B* 82, 125320 (2010).
34. S. Adachi, *Handbook on Physical Properties of Semiconductors: II–VI Compound Semiconductors*, vol. 3 (Kluwer, New York, 2004), p. 359.
35. A.M. Jagtap, J. Khatei, and K.S.R. Koteswara Rao, *Phys. Chem. Chem. Phys.* 17, 27579 (2015).
36. A.M. Jagtap, A. Chatterjee, A. Banerjee, N.B. Pendyala, and K.S.R. Koteswara Rao, *J. Phys. D Appl. Phys.* 49, 135302 (2016).
37. A.M. Kelley, *J. Phys. Chem. Lett.* 1, 1296 (2010).
38. D. Valerini, A. Cretí, M. Lomascolo, L. Manna, R. Cingolani, and M. Anni, *Phys. Rev. B* 71, 235409 (2005).
39. S. Rudin, T.L. Reinecke, and B. Segal, *Phys. Rev. B* 42, 11218 (1990).
40. F. Gindele, K. Hild, W. Langbein, and U. Woggon, *J. Lumin.* 87–89, 381 (2000).
41. M. Funato, K. Omae, Y. Kawakami, S. Fujita, C. Bradford, A. Balocchi, K.A. Prior, and B.C. Cavenett, *Phys. Rev. B* 73, 245308 (2006).
42. M. Nirmal, D.J. Norris, M. Kuno, M.G. Bawendi, A.L. Efros, and M. Rosen, *Phys. Rev. Lett.* 75, 3728 (1995).
43. T.G. Mack, L. Jethi, and P. Kambhampati, *J. Phys. Chem. C* 121, 28537 (2017).
44. D. Kushavah, P.K. Mohapatra, P. Ghosh, M. Singh, P. Vasa, D. Bahadur, and B.P. Singh, *Mater. Res. Express* 4, 075007 (2017).
45. J. Voigt, F. Spielgelberg, and M. Senoner, *Phys. Status Solidi B* 91, 189 (1979).
46. X. Wen, A. Sitt, P. Yu, Y.-R. Toh, and J. Tang, *Phys. Chem. Chem. Phys.* 14, 3505 (2012).
47. O. Schöps, N. Le Thomas, U. Woggon, and M.V. Artemyev, *J. Phys. Chem. B* 110, 2074 (2006).